

SUPPORTING INFORMATION:

Exploring the Potential of Tamoxifen-based Copper(II) Dichloride in Breast Cancer Therapy[†]

Aleksandr Kazimir,^a Benedikt Schwarze,^b Peter Lönnecke,^a Sanja Jelača,^c Sanja Mijatović,^c Danijela Maksimović-Ivanić,^c Evamarie Hey-Hawkins^{a*}

^aInstitute of Inorganic Chemistry, Faculty of Chemistry and Mineralogy, Leipzig University, Leipzig, Germany

^bInstitute of Medical Physics and Biophysics, Faculty of Medicine, Leipzig University, Germany

^cDepartment of Immunology, Institute for Biological Research "Siniša Stanković", National Institute of the Republic of Serbia, University of Belgrade; Bulevar despota Stefana 142, 11060 Belgrade, Serbia

* Correspondence:

Evamarie Hey-Hawkins

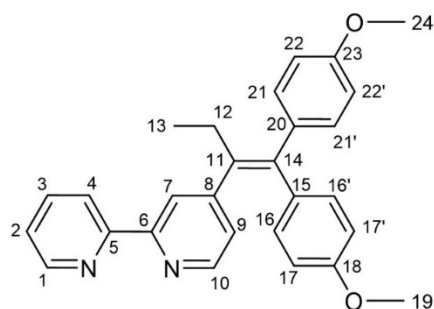
hey@uni-leipzig.de

[†] These results were presented in part at the 16th European Biological Inorganic Chemistry Conference: EuroBIC-16; 17-21 July 2022, Grenoble, France; abstract no. B11. <https://radar.ibiss.bg.ac.rs/handle/123456789/5318>

Table of Contents

1 Characterisation	3
1.1 4-[1,1-bis(4-methoxyphenyl)but-1-en-2-yl]-2,2'-bipyridine (L).....	3
1.2 [CuCl(μ -Cl)(L- κ^2N,N')] ₂	5
2 X-ray crystallography	7
2 UV-vis spectroscopy	8
3 Computational chemistry.....	11
3.1 Free energy of dissociation.....	12
3.2 Transitions.....	13
4 <i>In vitro</i> studies	16
5 References	17

1 Characterisation



1.1 4-[1,1-bis(4-methoxyphenyl)but-1-en-2-yl]-2,2'-bipyridine (L)

$M(C_{28}H_{26}Cl_2N_2O_2) = 422.53 \text{ g mol}^{-1}$. $^1\text{H NMR}$ (400 MHz, CDCl_3), δ (ppm): 8.67 (m, 1H, 1-CH), 8.40 (d, $^3J_{\text{HH}} = 8.6 \text{ Hz}$, 1H, 10-CH), 8.35 (d, $^3J_{\text{HH}} = 8.0 \text{ Hz}$, 1H, 4-CH), 8.30 (s, 1H, 7-CH), 7.80 (td, $^3J_{\text{HH}} = 7.8$, $^3J_{\text{HH}} = 1.8 \text{ Hz}$, 1H, 3-CH), 7.29 (ddd, $^3J_{\text{HH}} = 7.6$, $^3J_{\text{HH}} = 4.7$, $^4J_{\text{HH}} = 1.2 \text{ Hz}$, 1H, 2-CH), 7.16 (d, $^3J_{\text{HH}} = 8.5 \text{ Hz}$, 2H, 21,21'-CH), 6.93 (dd, $^3J_{\text{HH}} = 5.0$, $^4J_{\text{HH}} = 1.7 \text{ Hz}$, 1H, 9-CH), 6.89 (d, $^3J_{\text{HH}} = 8.6 \text{ Hz}$, 2H, 22, 22'-CH), 6.84 (d, 2H, $^3J_{\text{HH}} = 8.6 \text{ Hz}$, 2H, 16, 16'-CH), 6.56 (d, $^3J_{\text{HH}} = 8.6 \text{ Hz}$, 2H, 17, 17'-CH), 3.83 (s, 3H, 24-CH₃), 3.66 (s, 3H, 19-CH₃), 2.59 (q, $^3J_{\text{HH}} = 7.3 \text{ Hz}$, 2H, 12-CH₂), 0.97 (t, $^3J_{\text{HH}} = 7.4 \text{ Hz}$, 3H, 13-CH₃). $^{13}\text{C}\{^1\text{H}\}$ NMR (101 MHz, CDCl_3), δ (ppm): 158.6 (23-C), 158.0 (18-C), 156.3 (5-C), 155.9 (6-C), 152.3 (8-C), 149.1 (1-CH), 148.7 (10-CH), 140.2 (14-C), 138.7 (11-C), 136.9 (3-CH), 135.5 (20-C), 134.8 (15-C), 132.0 (16, 16'-CH), 130.5 (21,21'-CH), 125.8 (9-CH), 123.6 (2-CH), 121.3 (7-CH), 121.1 (4-CH), 113.6 (22, 22'-CH), 113.1 (17, 17'-CH), 55.3 (24-CH₃), 55.0 (19-CH₃), 28.4 (12-CH₂), 13.6 (13-CH₃). IR: 3050–2084 (w, Calk–H), 1604 (m, $\nu(\text{C}=\text{C})$), 1582 (m, $\nu(\text{C}=\text{C})$), 1537 (w, $\nu(\text{C}=\text{C})$), 1506 (s, $\text{C}_{\text{arom}}\text{-H}$ in-plane bending), 1458 (w, $\text{C}_{\text{arom}}\text{-H}$ in-plane bending), 1384 (w, $\text{C}_{\text{arom}}\text{-H}$ in-plane bending), 1292 (w), 1273 (w, $\text{C}_{\text{arom}}\text{-O}$), 1241 (s, $\text{C}_{\text{arom}}\text{-O}$), 1172 (s, $\text{C}_{\text{arom}}\text{-O}$), 1107 (m), 1069 (w), 1027 (s, Calk–O), 828 (m, out-of-plane bending), 792 (m, out-of-plane bending), 743 (s, out-of-plane bending), 724 (w), 661 (w), 627(w), 589 (w), 567 (w), 519 (w). **MS** (HR-ESI, pos.): $m/z = 423.2300$ (calc.: 423.2320; $[\text{M}+\text{H}]^+$); **Elemental analysis:** $\text{C}_{28}\text{H}_{26}\text{N}_2\text{O}_2 \cdot \text{H}_2\text{O}$ calc. (%) C 76.34, H 6.41, N 6.36; found (%) C 76.75, H 6.38, N 6.17.

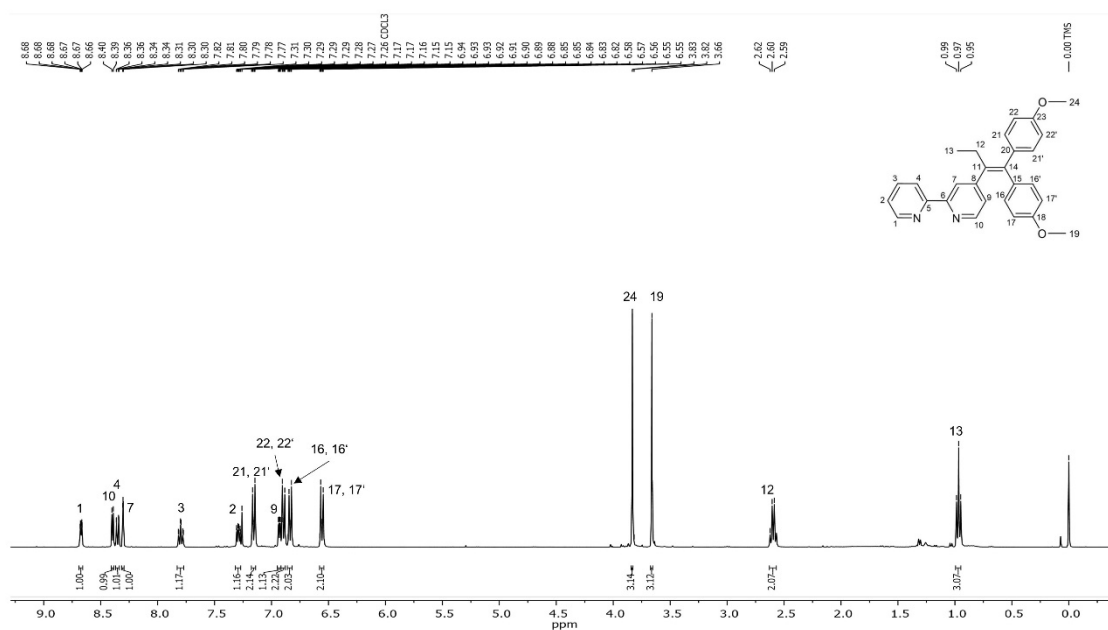


Figure S1. $^1\text{H NMR}$ spectrum of L in CDCl_3 .

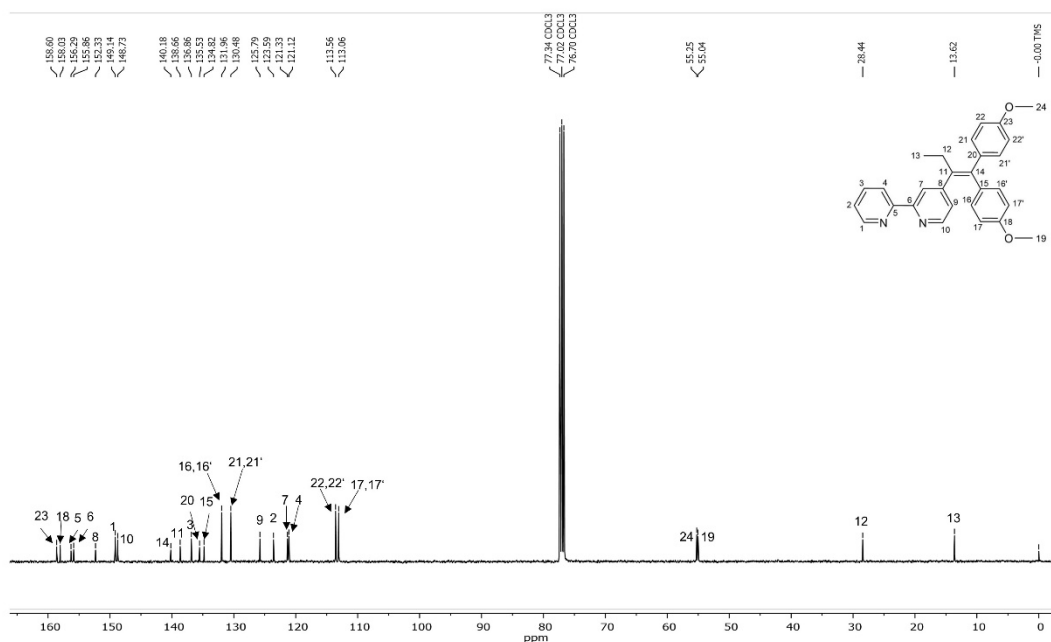


Figure S2. $^{13}\text{C}\{^1\text{H}\}$ NMR spectrum of **L** in CDCl_3 .

\\Users\guest...d\Result9-9.csv Injection 1 Function 1 MS + spectrum 0.00

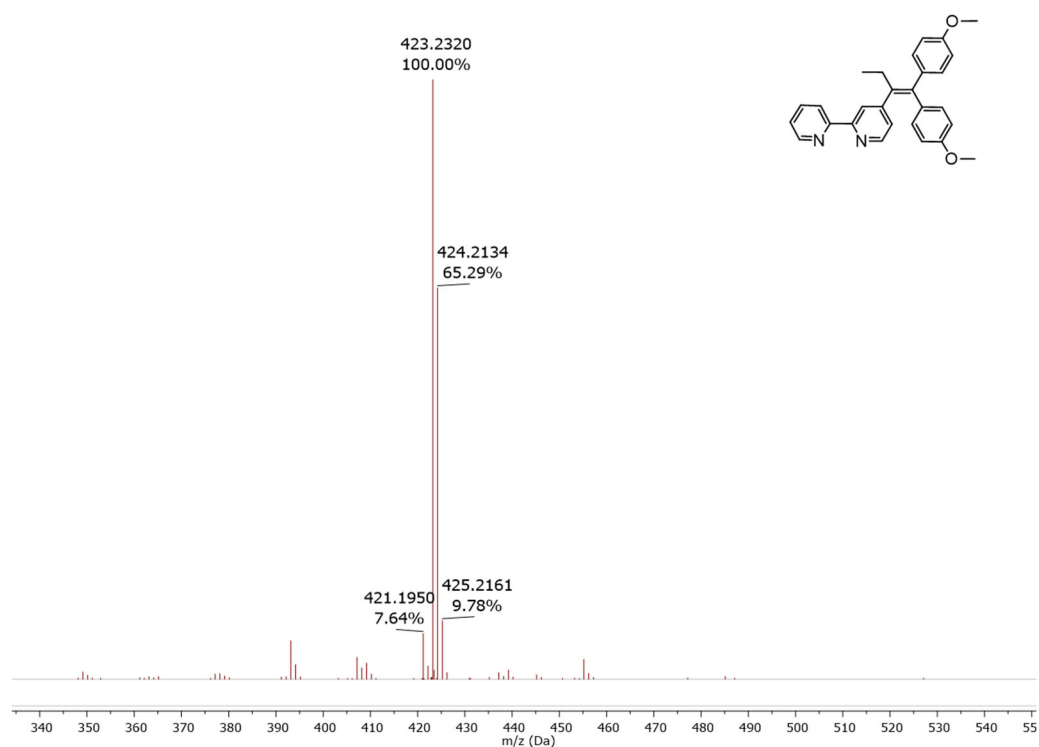


Figure S3. HR-ESI-MS (Positive mode, acetonitrile) of **L**: m/z $[\text{M}+\text{H}]^+$ = 423.2072 (calc.), 423.2320 (found).

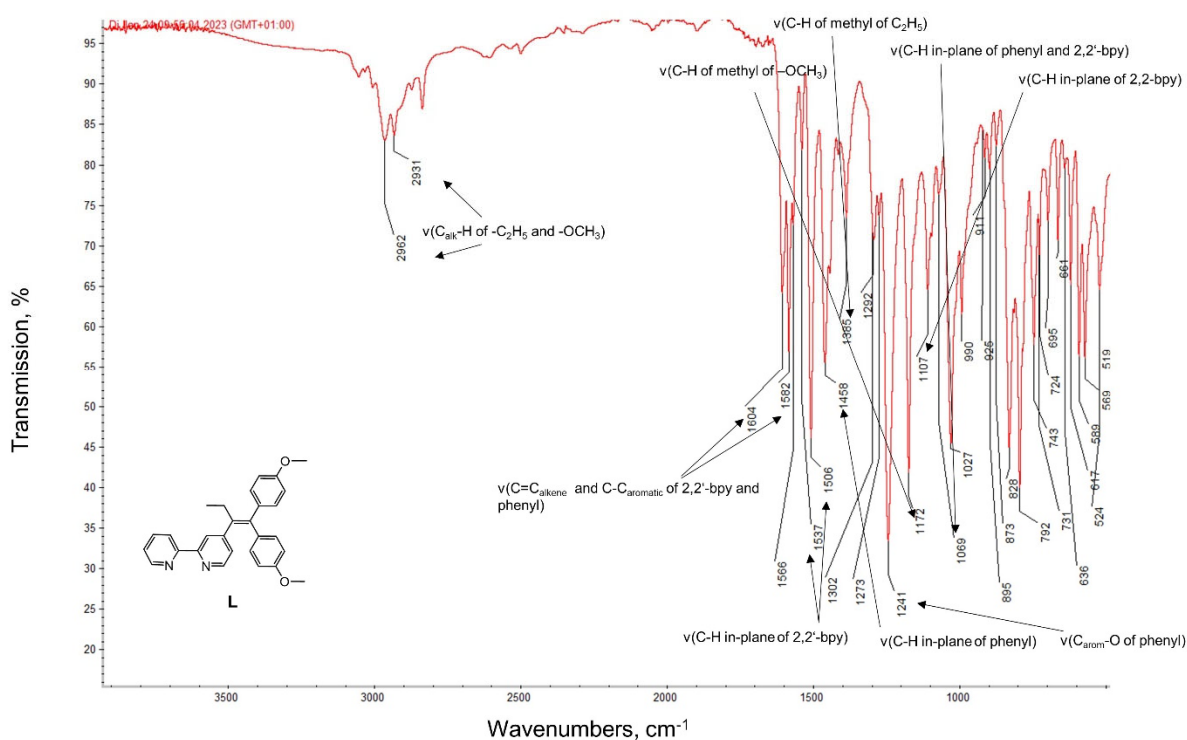


Figure S4. IR spectrum of **L**. The signals below 1107 cm^{-1} are assigned in Figure S7.

1.2 $[\text{CuCl}(\mu\text{-Cl})(\text{L}-\kappa^2\text{N},\text{N}')_2]$

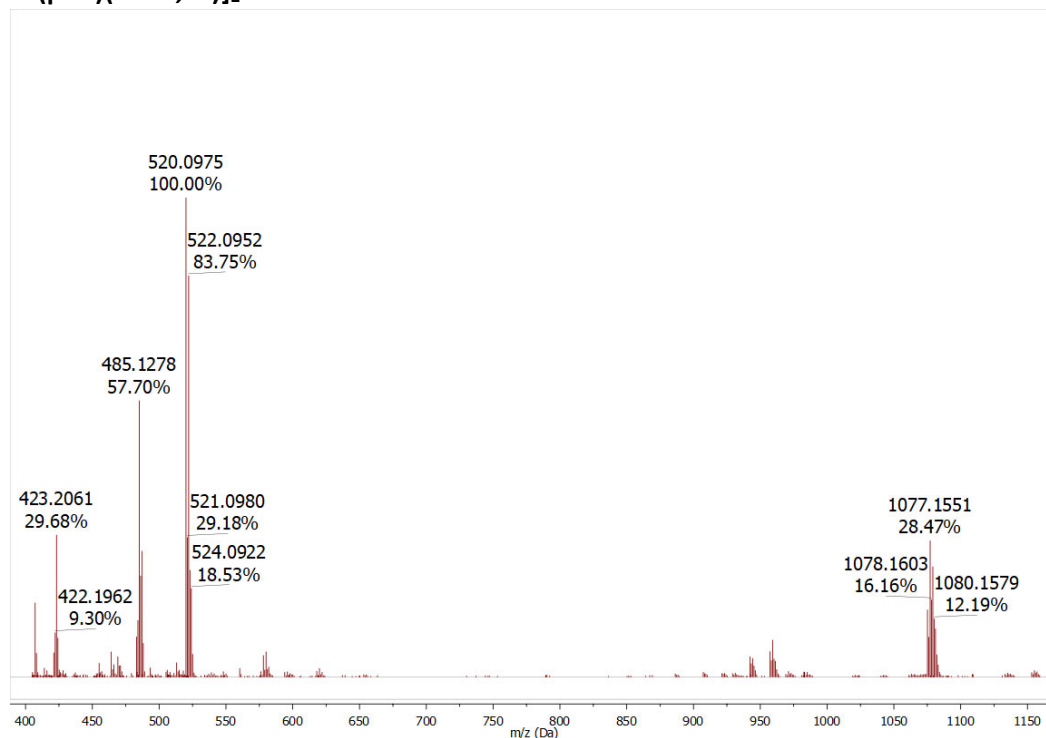


Figure S5. HR-ESI-MS (positive mode, acetonitrile) of **1**, $M = 1113.13\text{ g mol}^{-1}$: m/z $[\text{M}-\text{Cl}]^+ = 1077.1616$ (calc.), 1077.1551 (found); m/z $[(\text{M}/2)-\text{Cl}]^+ = 520.0979$ (calc.), 520.0975 (found); m/z $[(\text{M}/2)-2\text{Cl}]^+ = 485.1290$ (calc.), 485.1278 (found), m/z $[(\text{M}/2)-\text{CuCl}_2]^+ = 423.2073$ (calc.), 423.2061 (found).

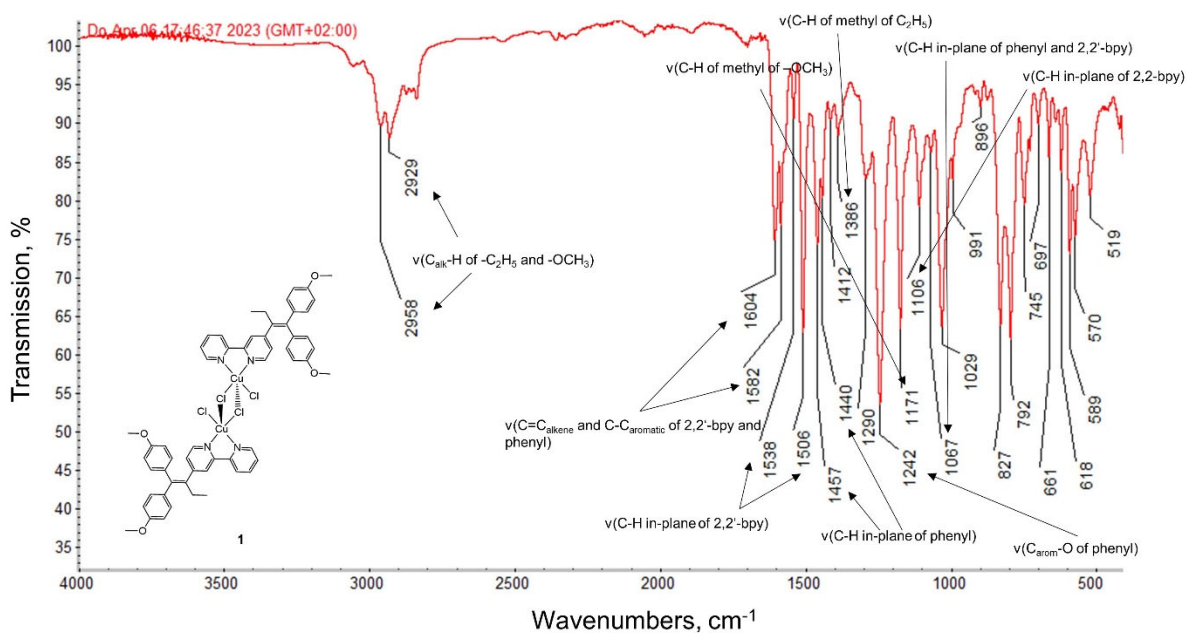


Figure S6. IR spectrum of $[\text{CuCl}(\mu\text{-Cl})(\text{L-}\kappa^2\text{N,N}')_2]$ (**1**). The signals below 1107 cm^{-1} are assigned in Figure S7.

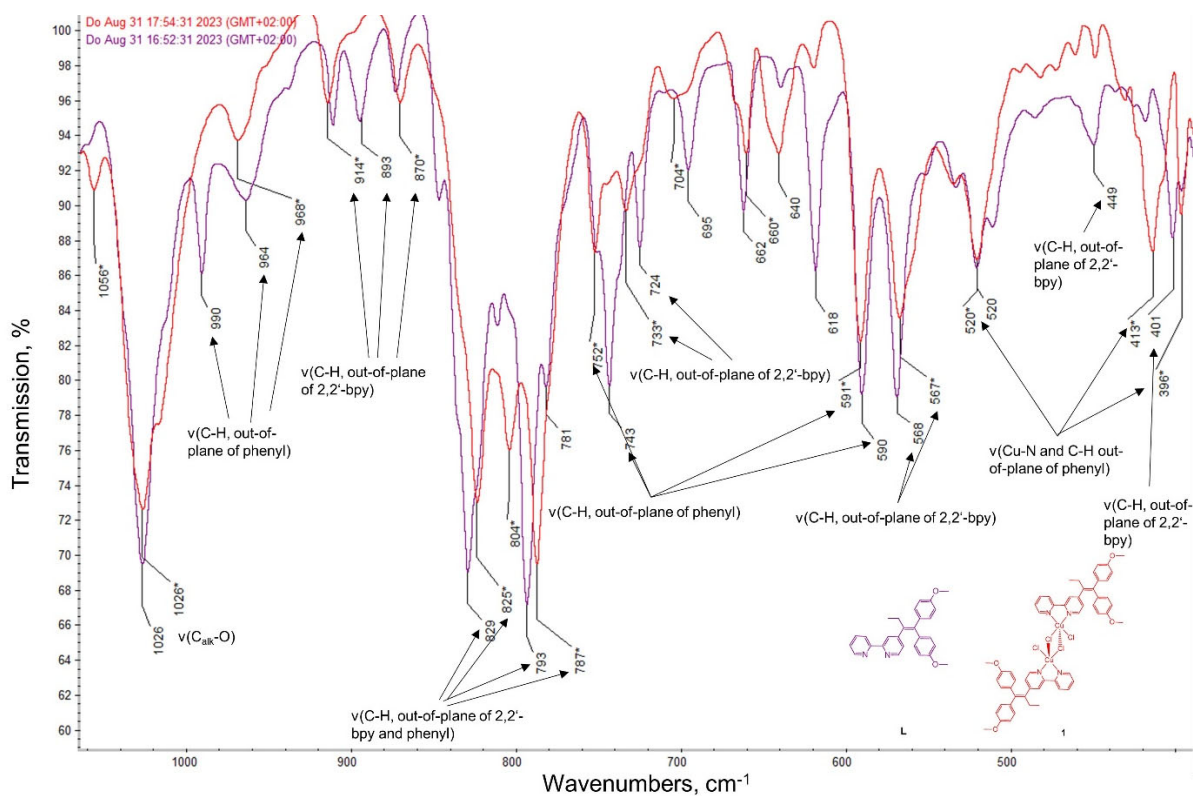


Figure S7. Overlapped IR spectra of $[\text{CuCl}(\mu\text{-Cl})(\text{L-}\kappa^2\text{N,N}')_2]$ (**1**, violet) and ligand (**L**, red). The assignment of the signals was supported by the calculated vibrations at PBE0 D3BJ/def2-TZVPP level of DFT.

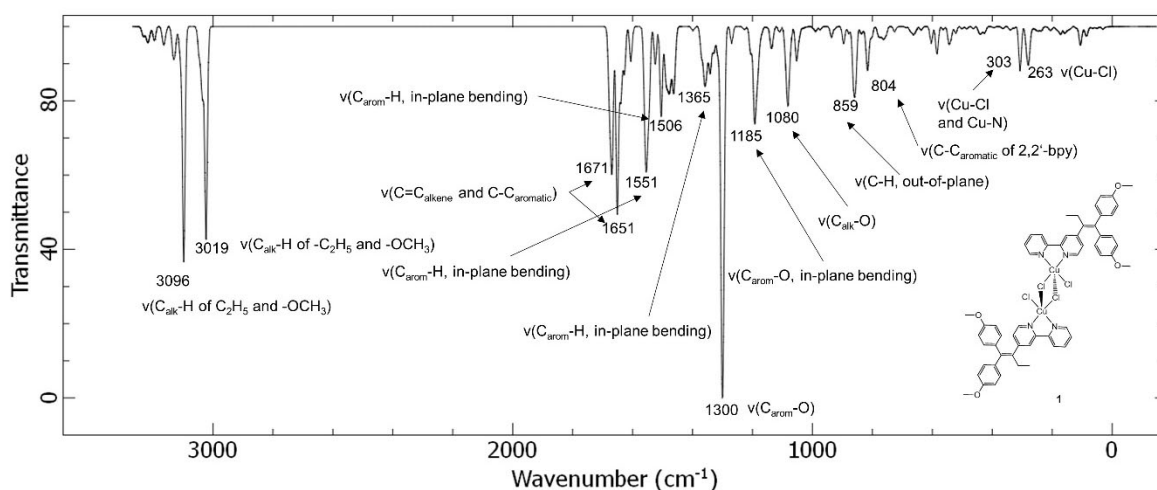


Figure S8. Calculated IR spectrum of $[\text{CuCl}(\mu\text{-Cl})(\text{L-}\kappa^2\text{N,N}')_2]$ (**1**) using DFT at PBE0 D3BJ/def2-TZVPP level of theory.

2 X-ray crystallography

The X-ray data (Table S1) were collected on a Gemini diffractometer (Rigaku Oxford Diffraction) using Mo-K α radiation and ω -scan rotation. Data reduction was performed with CrysAlisPro¹ including the program SCALE3 ABSPACK for empirical absorption correction. The structure was solved by dual space methods with SHELXT-2018² and the refinement was performed with SHELXL-2018³. With the exception of methyl substituents and disordered solvent molecules, all H atoms were located on difference Fourier maps calculated at the final stage of the structure refinement. The CH₂Cl₂ solvent molecules are disordered with a ratio of 0.911(3):0.089(2) (C29, Cl3, Cl4) and 0.862(2):0.138(2) (C30, Cl5, Cl6). Structure figures were generated with DIAMOND-4.⁴

The CCDC deposition number given in Table S1 contains the supplementary crystallographic data for this paper. The data can be obtained free of charge via <https://www.ccdc.cam.ac.uk/structures/> (or from the Cambridge Crystallographic Data Centre, 12 Union Road, Cambridge CB2 1EZ, UK; fax: (+44)1223-336-033; or deposit@ccdc.cam.ac.uk).

Table S1. Fundamental crystal structure parameters of $[\text{CuCl}(\mu\text{-Cl})(\text{L-}\kappa^2\text{N,N}')_2]$ (**1**).

Empirical formula	C ₆₀ H ₆₀ Cl ₁₂ Cu ₂ N ₄ O ₄
Molecular formula	C ₅₆ H ₅₂ Cl ₄ Cu ₂ N ₄ O ₄ · 4 CH ₂ Cl ₂
Formula weight	1453.60
Temperature	130(2) K
Wavelength	71.073 pm
Crystal system	Monoclinic
Space group	<i>P</i> 2 ₁ / <i>c</i>
Unit cell dimensions	a = 909.98(1), b = 1820.94(4), c = 1958.40(4) pm $\alpha = \gamma = 90^\circ$, $\beta = 90.433(2)^\circ$
Volume	3.2450(1) nm ³
Z	2
Density (calculated)	1.488 mg/m ³
Absorption coefficient	1.198 mm ⁻¹
<i>F</i> (000)	1484
Crystal size	0.50 x 0.05 x 0.05 mm ³

Theta range for data collection	2.080 to 32.430°
Index ranges	-12 ≤ h ≤ 11, -27 ≤ k ≤ 27, -29 ≤ l ≤ 26
Reflections collected	40802
Independent reflections	10857 [R(int) = 0.0446]
Completeness (theta)	100.0 % (30.51°)
Absorption correction	Semi-empirical from equivalents
Max. and min. transmission	1.00000 and 0.68223
Refinement method	Full-matrix least-squares on F^2
Data / restraints / parameters	10857 / 34 / 467
Goodness-of-fit on F^2	1.029
Final R indices [$I > 2\sigma(I)$]	R1 = 0.0545, wR2 = 0.1344
R indices (all data)	R1 = 0.0787, wR2 = 0.1484
Residual electron density	0.735 and -1.555 e·Å ⁻³
CCDC Number	2281073

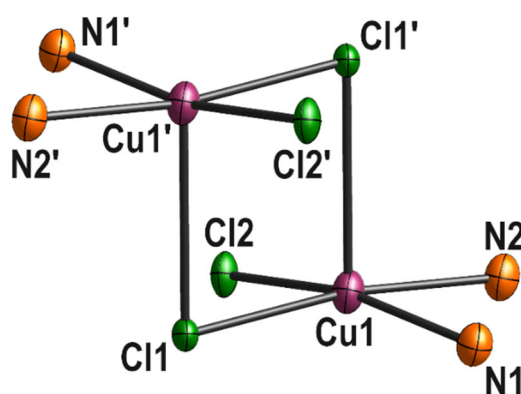


Figure S9. Central core of the dimeric complex $[\text{CuCl}(\mu\text{-Cl})(\text{L-}\kappa^2\text{N,N}')_2]$ (**1**) showing the square-pyramidal coordination environment at copper(II).

2 UV-vis spectroscopy

For the *in vitro* cell tests, the stock solution of the compound is typically prepared in DMSO and stored below 4 °C. For this purpose, the stability and solubility of the compound needs to be verified in DMSO/water solution with up to 1% (v/v) of DMSO. Therefore, a stock solution of **1** in DMSO was prepared (10 mM) and subsequently diluted 1:100 in deionised water. The mixture was stirred for 60 min before the first measurement. The solution was kept at 4 °C between the next measurements.

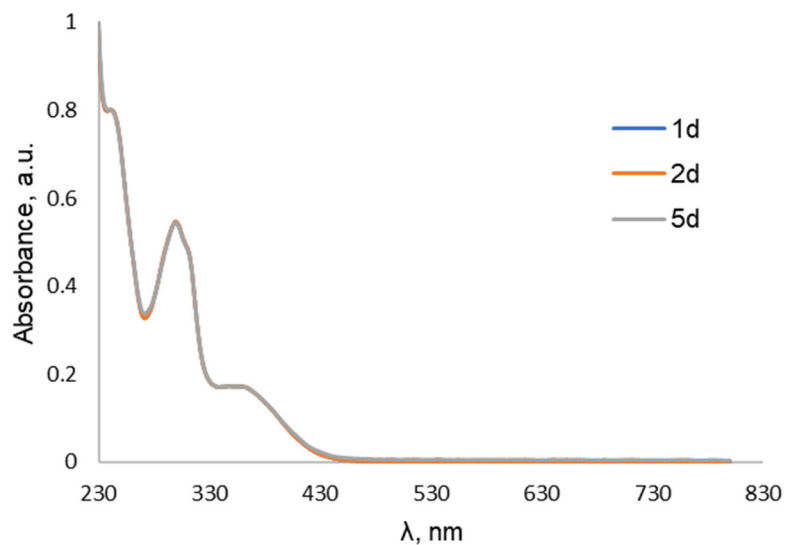


Figure S10. UV-vis spectra of **1** recorded in DMSO/water solution with 1% (v/v) of DMSO. No changes could be observed within 5 d.

The presence of coordinated water molecules in calculated monomeric complexes **2–4** (see chapter 3) was experimentally assessed by UV-vis spectroscopy by comparing the spectrum obtained for **1** in a non-coordinating solvent (dichloromethane) with spectra recorded in DMSO/water (1% v/v DMSO, Figure S10).

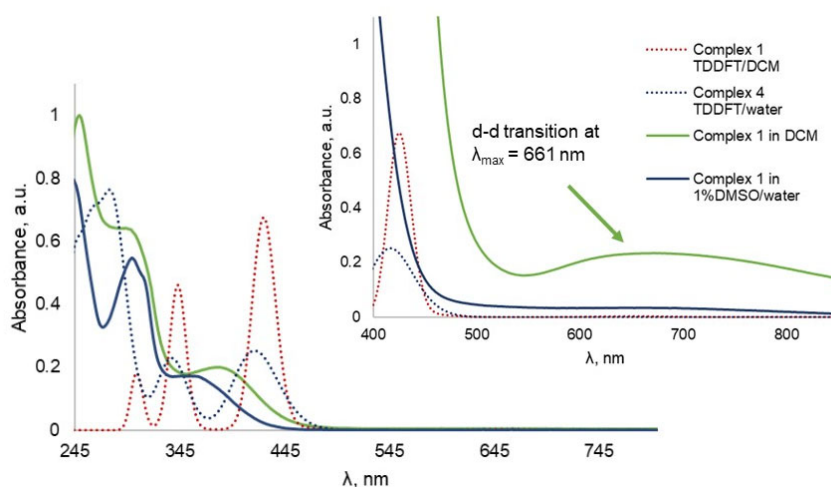


Figure S11. UV-vis spectra of compound **1** recorded in DCM (green line) and DMSO/water (with 1% (v/v) DMSO, dark blue line) and calculated (dotted lines) using TDDFT at PBE0 B3DJ/def2-TZVPP level of theory. The conductor-like polarisable model was used in this calculation to include the solvation effect (DCM, water). To observe the d-d transitions, the concentration of complex **1** was increased in both DCM and 1% DMSO/water solutions.

The d-d transition was observed in the non-coordinating solvent DCM, explaining the colour of the complex in the solution (green).

The **mole ratio method** was employed to obtain the stoichiometry of ligand:copper in solution. For this purpose, several solutions with the different ratios of ligand and copper dichloride ($\text{CuCl}_2 \cdot 2\text{H}_2\text{O}$) were prepared in ethanol in vials (2 ml) and kept stirring at room temperature over 12 hours. The

concentration of Cu^{2+} was maintained the same for all the solutions while the ligand concentration was varied. The absorbance was calculated at $\lambda_{\text{max}} = 372 \text{ nm}$ since at this wavelength we expect the overlap of two charge-transfer transitions (CTs), namely intraligand and ligand-to-metal (Figures S12 and S13).

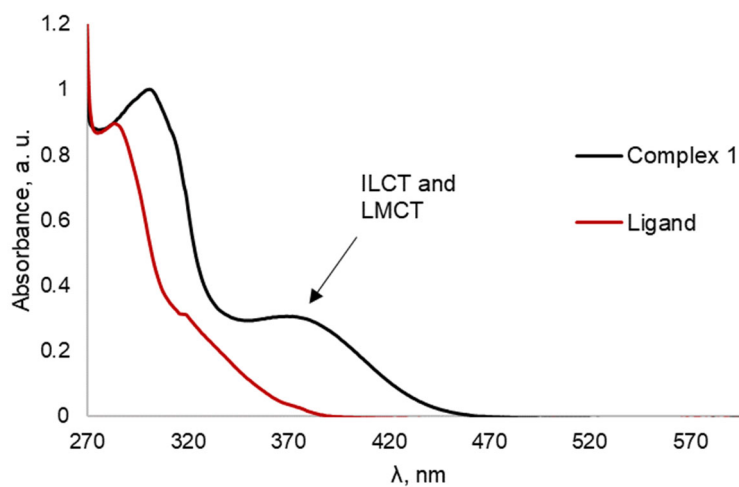


Figure S12. UV-vis spectra of complex **1** and ligand **L** recorded in ethanol.

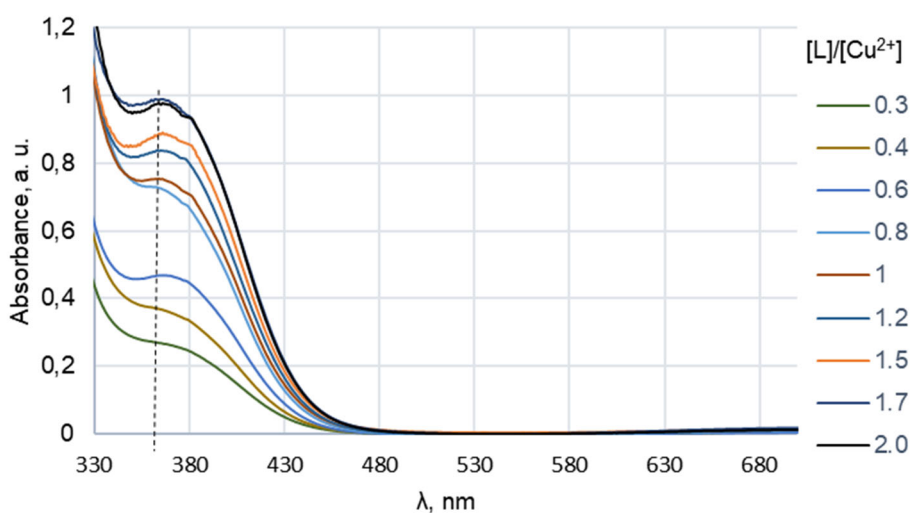


Figure S13. UV-vis spectra of the prepared solutions with the different ratios of ligand and copper ion $[\text{L}]/[\text{Cu}^{2+}]$ recorded in ethanol.

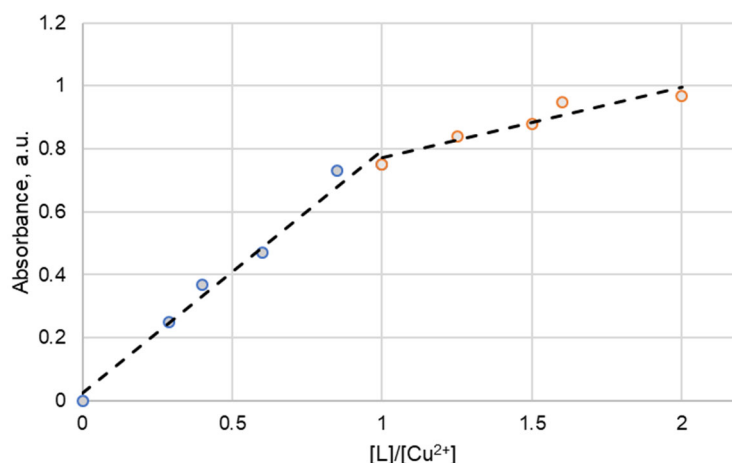


Figure S14. Absorption at $\lambda_{\max} = 372$ nm in the UV-vis spectra of the prepared solutions with different ratios of ligand and copper ion $[L]/[Cu^{2+}]$.

According to Figure S14, the proposed metal-to-ligand ratio in solution is 1:1.

3 Computational chemistry

The geometry optimisation of complex **1** was done based on X-ray crystal structures using density functional theory (DFT)⁶ and performed with the ORCA 5.0 package⁷. The monomeric species **2–4** were generated from the molecular structure of the dimeric form. The functional PBE0 has been chosen based on the results of benchmark studies for a set of the transition metal complexes.^{8,9} We have included Becke-Johnson dispersion correction of third order (D3BJ)¹⁰ in the functional. Additionally the density fitting technique resolution-of-identity approximation (RI-J)¹¹ and chain-of-sphere approximation (COSX)¹¹ were applied in the geometry optimisation to speed up the calculations. The polarised basis set def2-TZVPP¹² was applied for better convergence of the energy. The local minima of the optimised geometries were verified with numerical frequency analysis, where no imaginary frequencies were observed. The calculations of the excited states of both monomeric and dimeric complexes were performed using time-dependent DFT (TDDFT)⁵ at the similar level of theory including water or DCM as the conductor-like polarisable model (CPCM)¹³.

Table S2. Comparison of selected experimental bond lengths and angles of complex **1** with values calculated at the PBE0 D3BJ/def2-TZVPP level of theory.

Bond or angle	Bond length or bond angle (exp.)	Bond length or bond angle (calc.)
Cu1–Cl1	229.87(6) pm	229.1 pm
Cu1–N1	203.5(2) pm	204.3 pm
Cu1–Cl2	225.10(6) pm	227.8 pm
Cu1–N2	201.6(2) pm	201.9 pm
N2–Cu1–Cl2	93.61(6)°	94.4°
N1–Cu1–Cl1	93.86(6)°	93.9°
Cl2–Cu1–Cl1	91.33(2)°	92.3°
N1–Cu1–N2	79.81(8)°	80.1°
Cl2–Cu1–Cl1'	100.0°	104.4°
Cl1–Cu1–Cl1'	89.69(2)°	92.4°

3.1 Free energy of dissociation

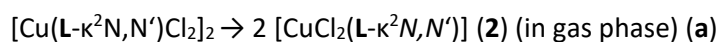
Table S3. Absolute free energies of dimeric and possible monomeric species in the gas phase and water.

Structure	Phase	Absolute free energy G, a.u.
4-[1,1-bis(4-methoxyphenyl)but-1-en-2-yl]-2,2'-bipyridine (L)	Gas	-1263.4211
	Water	-1263.4709
[CuCl(μ-Cl)(L-κ ² N,N')] ₂ (1)	Gas	-7803.3602
	Water	-7803.4320
[CuCl ₂ (L-κ ² N,N')] (2)	Gas	-3901.0126
	Water	-3901.0624
[CuCl(L-κ ² N,N')] ⁺	Gas	-3441.3495
[Cu(L-κ ² N,N')] ²⁺	Water	-2981.1815
[CuCl(L-κ ² N,N')(H ₂ O)] ⁺	Water	-3517.1772
[CuCl ₂ (L-κ ² N,N')(H ₂ O)] (3)	Water	-3978.0871
[CuCl ₂ (L-κ ² N,N')(H ₂ O) ₂] (4)	Water	-4054.4646
H ₂ O	Water	-76.3735
Cu ²⁺	Water	-1717.6901
Cl ⁻	Gas	-460.1324
Cl ⁻	Water	-460.2515

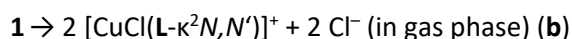
ΔG of dissociation was calculated according to:

$$\Delta G = \sum_i^{i=n} \nu_i G_i (\text{products}) - \sum_i^{i=n} \nu_i G_i (\text{reactants}) \quad (1)$$

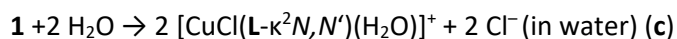
Examples of calculations:



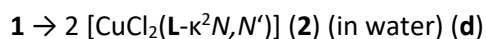
ΔG = 2 · (-3901.0126) - (-7803.3602) = 1.34 a. u. (3505 kJ mol⁻¹)



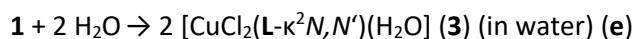
ΔG = 2 · (-3441.3495) + 2 · (-460.1324) - (-7803.3602) = 0.40 a. u. (1041 kJ mol⁻¹)



ΔG = 2 · (-3517.1772) + 2 · (-460.2515) - (-7803.4320) - 2 · (-76.3735) = 1.32 a. u. (3470 kJ mol⁻¹)



ΔG = 2 · (-3901.0624) - (-7803.4350) = 1.31 a. u. (3440 kJ mol⁻¹)



ΔG = 2 · (-3978.0871) - (-7803.4320 + 2 · (-76.3735)) = 0.0048 a. u. (12.6 kJ mol⁻¹)

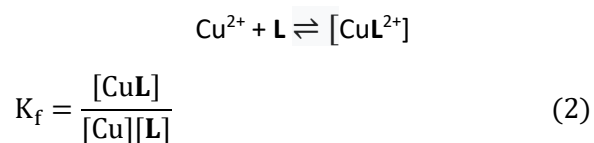


ΔG = 2 · (-4054.4646) - (-7803.4320 + 4 · (-76.3735)) = -0.0032 a. u. (-8.4 kJ mol⁻¹)

Complex [CuCl₂(L-κ²N,N')(H₂O)₂] (**4**) exhibited the lowest free energy (G) and displayed an octahedral configuration, indicating its high stability. The negative energy of dissociation (-8.4 kJ mol⁻¹) suggests the formation of this monomeric complex in aqueous solution. Interestingly, although the gas-phase dissociation showed a positive free energy of dissociation (1041 kJ mol⁻¹) for the formation of [CuCl(L-

κ^2N,N']⁺ ions, the mass spectra showed the presence of these ions. This suggests that factors such as ionisation and experimental conditions beyond thermodynamics may play essential roles in the formation of this dissociated species.

In order to calculate the stability constant of the copper complex in water solution we followed the next scheme:



Where K_f can be calculated from the equation: $\Delta G = -RT \ln K_f$ and ΔG was calculated in accordance with eq. 1. $\Delta G = (-2981.1815) - (-1263.4709 + (-1717.6901)) = -0.0205$ a. u. (-54 kJ mol^{-1}).

The stability constant $K_f = e^{-\Delta G/RT}$ at 298 K is $1.14 \cdot 10^9$ confirming the high stability of compound **1** in water solution.

3.2 Transitions

Table S4. One-electron HOMO-LUMO transitions and many-electron charge transfer (CT) transitions proceeding at the curtain wavelength as intra-ligand CT (ILCT), ligand-to-metal CT (LMCT) and $d-d$ transitions. Only HOMO-LUMO transitions with the highest contributions in CTs were considered.

Complex	λ_{max} , nm	HOMO-LUMO	Type of transition
[CuCl(μ -Cl)(L- κ^2N,N')] ₂ (1)	304	HOMO-6 → LUMO+1	ILCT (Ph → 2,2'-bpy), LMCT (Cl → Cu)
	344	HOMO-2 → LUMO	ILCT (Ph → 2,2'-bpy)
	425	HOMO-2 → LUMO+2	LMCT (Ph → [CuCl ₂])
	666	HOMO-7 → LUMO+2	$d-d$ transition (Cu)
[CuCl ₂ (L- κ^2N,N')(H ₂ O) ₂] (4)	262	HOMO-3 → LUMO	ILCT (Ph → 2,2'-bpy), LMCT (Cl/H ₂ O → Cu)
	338	HOMO-1 → LUMO+1	ILCT (Ph → 2,2'-bpy)
	416	HOMO-1 → LUMO	ILCT (Ph → 2,2'-bpy), LMCT (Cl → Cu)
	631	HOMO-5 → LUMO+2	$d-d$ transition (Cu)

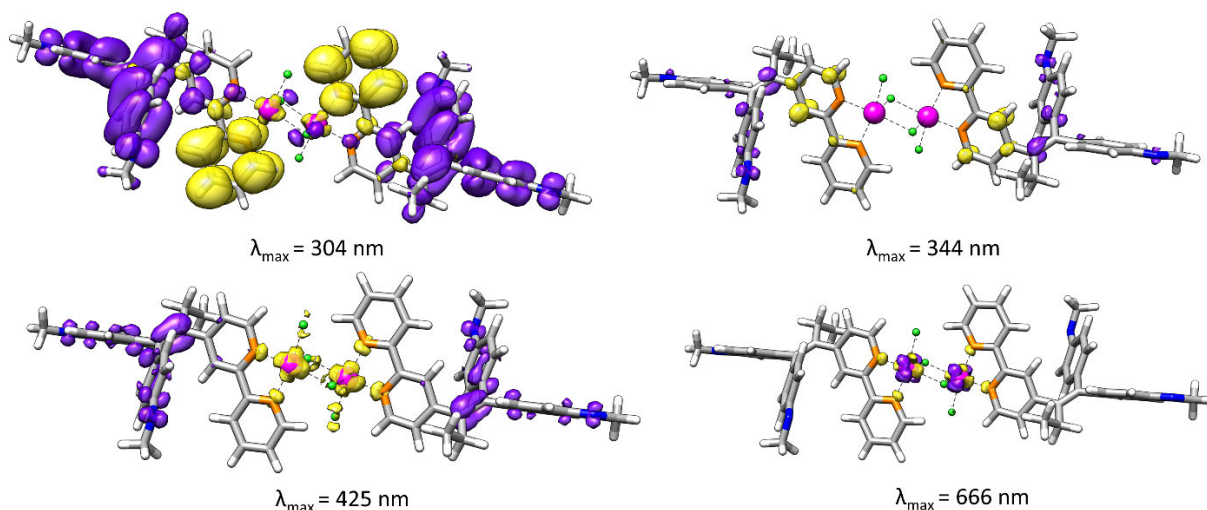


Figure S15. Difference densities of **1** visualising the charge transfer (CT) at certain wavelengths proceeding from purple to yellow iso-surfaces (iso-value = 0.004). The iso-value for $\lambda_{\max} = 304 \text{ nm}$ was decreased in order to observe the contribution of Cu and Cl in this CT (iso-value = 0.0002).

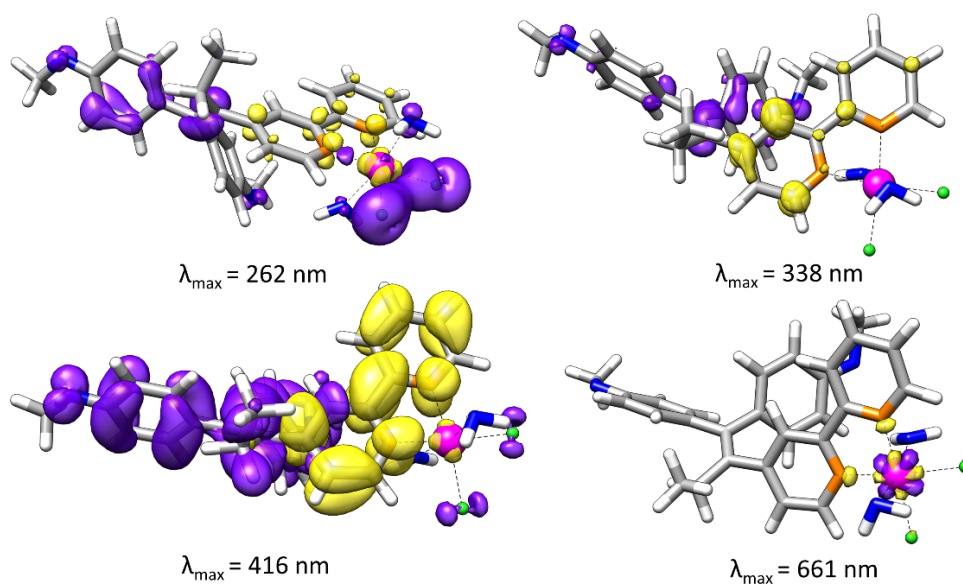


Figure S16. Difference densities of **4** visualising the charge transfer at certain wavelengths proceeding from purple to yellow iso-surfaces (iso-value = 0.004). The iso-values for $\lambda_{\max} = 262 \text{ nm}$ and $\lambda_{\max} = 416 \text{ nm}$ were decreased in order to observe the contribution of Cu, Cl and H₂O in this CT (iso-value = 0.0002).

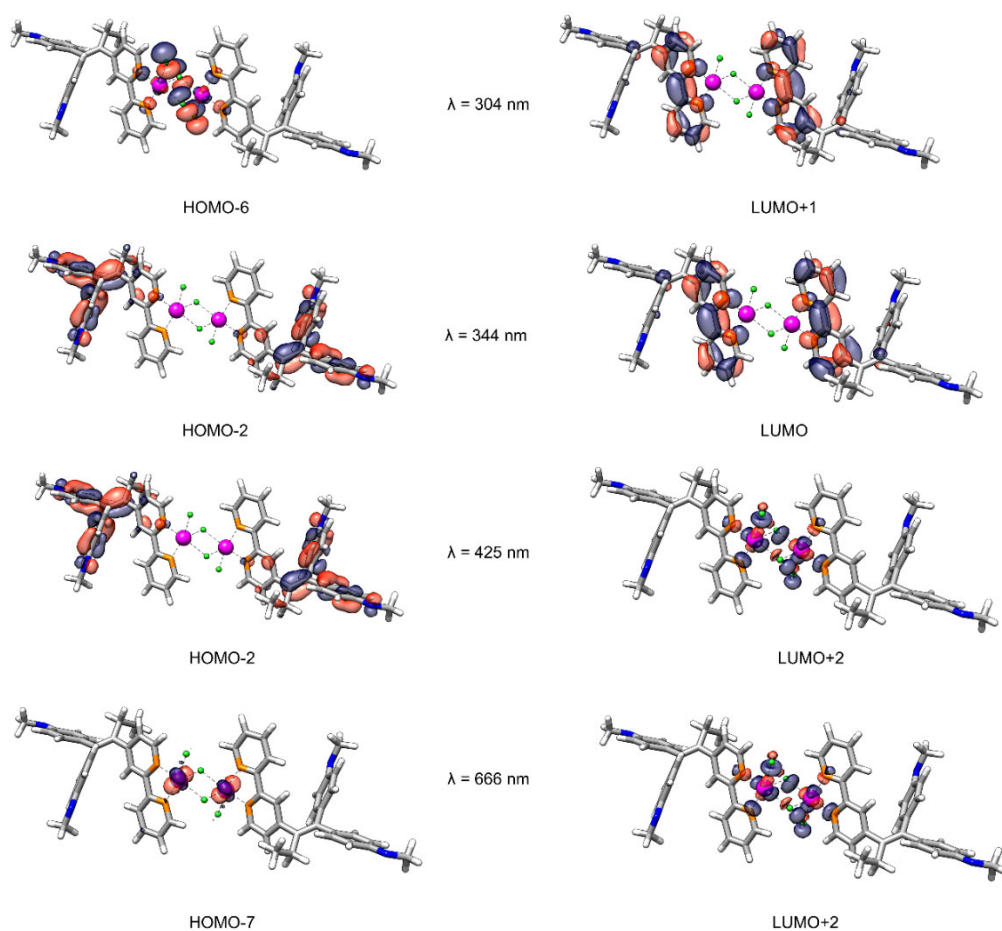


Figure S17. Molecular orbitals involved in HOMO-LUMO transitions of **1** visualising the one-electron transitions at certain wavelengths (iso-value = 0.03).

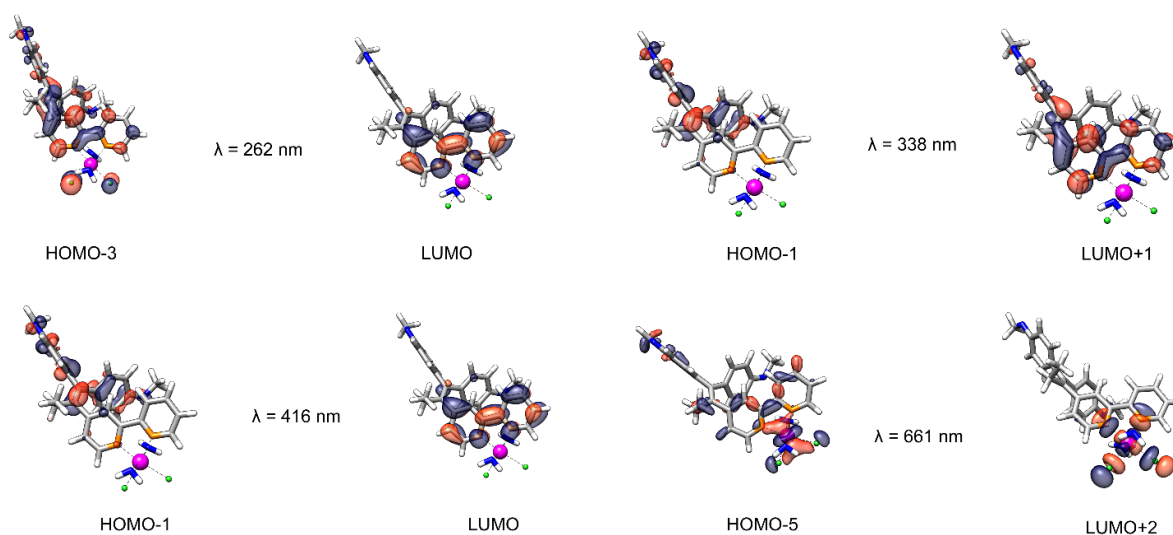


Figure S18. Molecular orbitals involved in HOMO-LUMO transitions of **4** visualising the one-electron transitions at certain wavelengths (iso-value = 0.03).

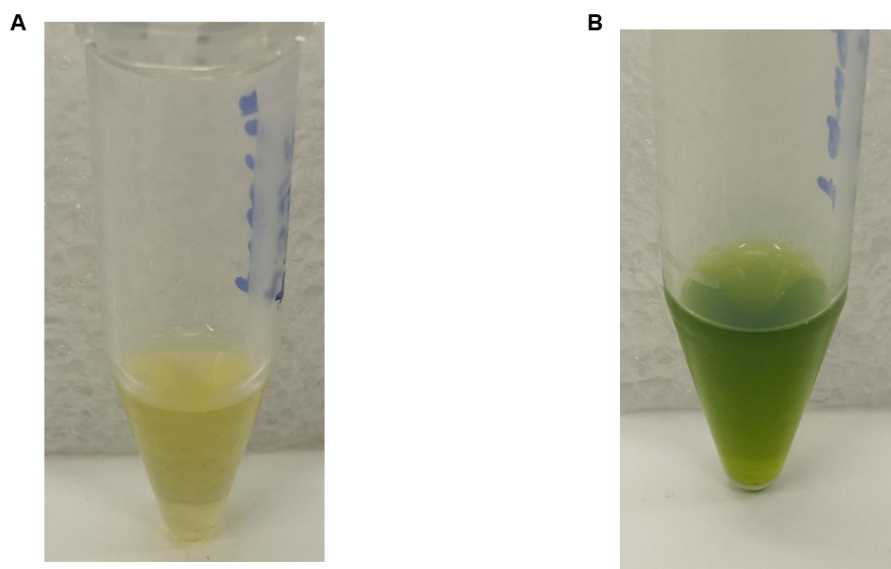


Figure S19. Solution of the ligand **L** (pale yellow, **A**) and solution of the copper complex **1** (green, **B**) in DCM.

4 *In vitro* studies

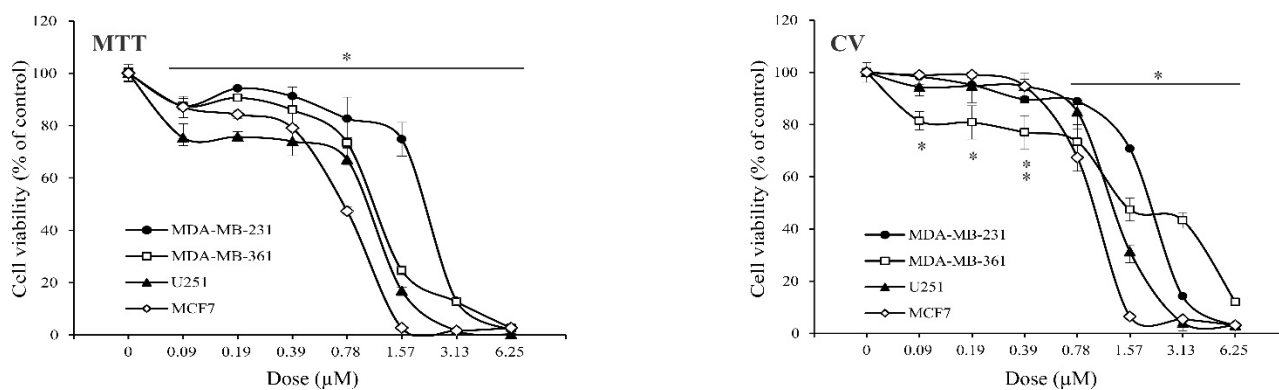


Figure S20. Compound **1** reduced the viability of cancer cells in a dose-dependent manner. Cells were treated with compound **1** in concentrations ranging from 0 to 6.25 μM for 72 h. Cell viability was determined by the MTT and CV tests. The data are presented as a mean ± SD from one representative out of three independent experiments. * $p < 0.05$ refer to untreated cultures.

5 References

- 1 Rikagu Oxford Diffraction. CrysAlisPro; Agilent Technologies inc.: Yarnton, Oxfordshire, UK, 2018, <https://www.rigaku.com/products/crystallography/crysalis>, (accessed 2 January 2023).
- 2 G. M. Sheldrick, *Acta Crystallogr. Sect. Found. Adv.*, 2015, **71**, 3–8.
- 3 G. M. Sheldrick, *Acta Crystallogr. Sect. C Struct. Chem.*, 2015, **71**, 3–8.
- 4 C. F. Macrae, I. Sovago, S. J. Cottrell, P. T. A. Galek, P. McCabe, E. Pidcock, M. Platings, G. P. Shields, J. S. Stevens, M. Towler and P. A. Wood, *J. Appl. Crystallogr.*, 2020, **53**, 226–235.
- 5 E. Runge and E. K. U. Gross, *Phys. Rev. Lett.*, 1984, **52**, 997–1000.
- 6 W. Kohn, in *Density Functional Methods In Physics*, eds. R. M. Dreizler and J. da Providência, Springer US, Boston, MA, 1985, pp. 1–9.
- 7 F. Neese, *WIREs Comput. Mol. Sci.*, 2012, **2**, 73–78.
- 8 C. J. Cramer and D. G. Truhlar, *Phys. Chem. Chem. Phys.*, 2009, **11**, 10757–10816.
- 9 T. Weymuth, E. P. A. Couzijn, P. Chen and M. Reiher, *J. Chem. Theory Comput.*, 2014, **10**, 3092–3103.
- 10 H. Schröder, A. Creon and T. Schwabe, *J. Chem. Theory Comput.*, 2015, **11**, 3163–3170.
- 11 S. Kossmann and F. Neese, *J. Chem. Theory Comput.*, 2010, **6**, 2325–2338.
- 12 A. Hellweg and D. Rappoport, *Phys. Chem. Chem. Phys.*, 2014, **17**, 1010–1017.
- 13 A. V. Marenich, C. J. Cramer and D. G. Truhlar, *J. Phys. Chem. B*, 2009, **113**, 6378–6396.